Universiteit Leiden
The Netherlands

Platinum surface instabilities and their impact in electrochemistry

Valls Mascaro, F.

Citation
Valls Mascaro, F. (2024, September 5). *Platinum surface instabilities and their impact in electrochemistry*. Retrieved from https://hdl.handle.net/1887/4054933

Version:	Publisher's Version
License:	Licence agreement concerning inclusion of doctoral thesis in the Institutional Repository of the University of Leiden
Downloaded from:	https://hdl.handle.net/1887/4054933

Note: To cite this publication please use the final published version (if applicable).

4 Quantitative Study of Electrochemical Adsorption and Oxidation on Pt(111) and its Vicinal Surfaces

Hydrogen and oxygen are key intermediates in many relevant electrochemical reactions such as the hydrogen oxidation and the oxygen reduction on platinum, which are the main processes in hydrogen fuel cells. Achieving improved catalyst design requires thus a deep understanding of their adsorption behavior. However, the interaction of hydrogen and oxygen with platinum step sites remains relatively limited, despite extensive fundamental research on their adsorption on platinum terraces. Our results show that the voltammetric peak related to hydrogen desorption from steps involves more than the simple desorption of one hydrogen atom per unit step length, which could point out towards an exchange mechanism between hydrogen and hydroxide, as stated in recent literature. At higher potentials, a one-dimensional surface oxide consisting of PtO_2 chains forms along the steps, giving rise to three voltammetric peaks that we relate to specific surface sites. Finally, we show that the adsorption of both hydrogen and oxygen is less pronounced at step bunches than at single steps, which we attribute to structural differences.

4.1 Introduction

The platinum-electrolyte interface is probably the most fundamentally studied system in electrocatalysis due to its relevance in electrochemical applications such as electrolyzers and fuel cells. Of special interest is the adsorption/desorption of hydrogen and oxygen on the platinum surface. The former has a crucial role in the hydrogen evolution and the hydrogen oxidation reaction [1–3], while the latter is a key intermediate in the oxygen reduction reaction (ORR) [4] as well as in oxidation reactions catalyzed by platinum [5].

The electrosorption of hydrogen on platinum starts at a potential more positive than the equilibrium potential for water reduction (or protons in acidic media) and thus it is often referred to as the *underpotential deposition* (upd) of hydrogen [1,6], H_{upd}, in analogy to the well-known upd of metals in electrodeposition [7,8]. The development of flame-annealing for single crystal preparation [9] allowed to probe the H_{upd} on well-defined crystallographic planes. These studies concluded that the hydrogen adsorption on platinum is surface specific (i.e. the adsorption energy depends on the coordination of the adsorption site) [10,11], which explained the differences observed in the respective Cyclic Voltammograms (CVs) of the low Miller-index planes: (111), (100), and (110) [12,13]. Not surprisingly, stepped platinum surfaces (vicinal to the low Miller-index planes) exhibit specific peaks in the H_{upd} *fingerprint*, allowing not only the differentiation between terrace and step contributions but also between different types of steps [14–16]. Nevertheless, recent studies support that these step peaks do not involve simple hydrogen adsorption/desorption, as it is the case on the terraces, but a replacement mechanism in which also hydroxide participates [17,18]. The details of this exchange process are still not fully understood.

Similarly to the above, the precise oxide structure at steps during platinum oxidation remains also unclear. The reason here is the complexity of this process: it involves multiple reaction steps [19], different surface oxidation states [20], and the so-called *place-exchange*, where platinum atoms are lifted up to a complete monolayer (ML) by oxygen atoms that go subsurface [21–27]. The first studies ignored the geometry effect of the adsorption sites and attributed the different oxidation peaks in the CV to different surface oxides, such as PtOH and PtO [28]. This picture was improved by Björling et al., who concluded that the multiple peaks in the oxidation region are likely due to the oxidation of different surface sites, such as terrace and step sites, with unique atomic arrangements [29,30]. Unraveling the oxide structure at the steps is of crucial importance, as the coverage of oxygenated species such as OH_{ad} and O_{ad} determines the ORR activity as well as the oxidation of organic molecules [4,5,31–34]. Moreover, it is known that surface oxidation is responsible for electrode degradation [35,36].

Furthermore, we recently proved with Electrochemical Scanning Tunneling Microscopy (EC-STM) that flame-annealed (111)-vicinal surfaces with terraces equal or narrower than Pt(775) are not stable and undergo step bunching, a well-known phenomenon in surface science (see Chapter 3) [37,38]. Additionally, we showed that these structural changes alter the reactivity of steps towards relevant surface-sensitive reactions such as the ORR. Therefore, also the hydrogen and oxygen adsorption on these unstable surfaces needs to be revisited.

To address these issues, here we deconvolute the terrace and step contributions in both the H_{upd} and the oxidation region. We quantify our analysis by extracting the corresponding step charge densities. Our results show that the H_{upd} step contribution involves more charge than the one corresponding to the desorption of one hydrogen atom per unit step length. This could point out towards a replacement mechanism between H_{ad} and OH_{ad} at the step sites, as stated in previous studies [17, 18]. Regarding the oxide, we present evidence from the coverage that the steps form PtO_2 rows, which agrees with previous work [39–42]. Finally, we demonstrate a decrease of the hydrogen and oxygen adsorption on bunched stepped surfaces, which we ascribe to the loss of step sites due to bunching.

4.2 Experimental

The CVs were recorded in a three-electrode glass cell that underwent sequential cleaning: first with an acidic potassium permanganate solution, then with diluted piranha, and finally by boiling it five times in ultrapure water (> 18.2 MΩ cm, Millipore, Milli-Q). We used a reversible hydrogen electrode (RHE) as reference electrode and a Pt wire (MaTeck, Germany) as counter. For the measurements we used a Pt(111) single crystal (Surface Preparation Laboratory, The Netherlands) and different (111)-vicinal surfaces with <110>/{111} steps (MaTeck, Germany): steps along a direction equivalent to [110] with {111} microfacets. In particular we used Pt(15 15 14), Pt(554), Pt(775), Pt(553), and Pt(221), which have nominal terrace widths of n = 30, 10, 7, 5, and 4 atomic rows, respectively. Prior to each experiment, the corresponding sample was etched electrochemically (125 cycles at 50 Hz and ± 2 V versus Pt) in an acidified 2.5 M $CaCl_2$ solution, flame annealed (3 min at ≈1250 K), and then cooled down in a 1:4 H_2/Ar mixture. We repeated this treatment at least three times before an experiment, performing the last annealing step to a slightly lower temperature (≈ 50 K lower) in order to create a denuded zone near the surface with less contamination. All the CVs were recorded in a dearated 0.1 M $HClO_4$ solution (Merck Suprapur) at a scan rate of 50 mV/s, using a potentiostat from Bio-Logic (VSP-300).

To correct for the surface miscut angle, we calculated all current and charge densities by using the electrochemical area (A_{ec}), which for stepped surfaces differs from the geometrical area (A_{geom}) according to:

$$A_{ec} = \frac{A_{geom}}{cos(\alpha)} \tag{4.1}$$

in which α is the angle of misorientation of the surface with respect to the (111) plane.

4.3 Cyclic Voltammetry of (111)-Vicinal Surfaces with (111) Steps

Figure 4.1 shows the CVs of Pt(111) and selected (111)-vicinal surfaces with (111) steps, recorded in 0.1 M $HClO_4$ between 0.06 and 1.35 V at a scan rate of 50 mV/s. The general trends of local changes in the CVs due to an increase of step density are indicated with black arrows. The broad feature below 0.4 V, attributed to hydrogen adsorption/desorption

at terrace sites [3,14], becomes narrower with increasing step density, indicating a decrease in entropy of the adsorbed hydrogen atoms [8,43]. Moreover, there is a sharp peak related to the (111) step sites at around 0.128 V [44–46]. In addition, Pt(553) and Pt(221) exhibit an extra hydrogen peak at around 0.18 V that is only observed on platinum stepped surfaces with narrow terraces [47]. In Chapter 3 we presented evidence from EC-STM measurements that this is attributed to hydrogen adsorption/desorption (and its partial exchange with hydroxide) at step bunches, which are only present on (unstable) surfaces with high step density.

The presence of steps also alters the adsorption of hydroxide in the so-called butterfly peak, the onset of which shifts from 0.55 V for Pt(111), to 0.62 V for Pt(221). In addition, the sharp OH peak decreases in height and becomes broader, indicating a suppression of the phase transition that results in an ordering of the OH adlayer [48]. Without the presence of steps, the region between 0.85 V and 1.0 V shows a flat plateau that is a consequence of a kinetic barrier for the formation of surface oxide on flat terraces [19,49–51]. On (111)-vicinal surfaces, however, this region is characteristic for step oxidation, explaining the presence of the voltammetric peaks observed [30,51]. The fact that step sites oxidize at lower potentials than terrace sites agrees well with theoretical calculations [40–42,52], which show that the oxygen atoms bind stronger at steps.

The peak at around 1.1 V is attributed to the conversion of OH_{ad} to O_{ad} on the terraces [19,49,53] and the Reversible Place-Exchange (PE_{rev}) between O_{ad} and platinum surface atoms [26,27,51,54–57]. This process results in platinum atoms being lifted out of the surface by almost one atomic layer due to the subsurface migration of oxygen atoms (i.e. two oxygen atoms go subsurface beneath one platinum atom involved) [26,56,57]. As the PE_{rev} is a precursor to the terrace oxidation [51], its voltammetric peak decreases in intensity when diminishing the number of terrace sites. Moreover, the PE_{rev} peak becomes broader and shifts its position with increasing step density (narrower terraces), which must be due to Smoluchowski relaxations changing the inter-atomic distances in the terrace [58–61]. Increasing the electrode potential above ≈ 1.17 V leads to the Irreversible Place-Exchange (PE_{irr}) [26,27,54,56,62], which ultimately results in the roughening of the surface due to the formation of nanoislands [27,51,57,63–65].

4.4 Adsorption of Hydrogen and Hydroxide at Step Sites

Clavilier and co-workers have previously found that the charge under the peak at around 0.128 V scales linearly with the step density, with 1 electron per unit step length, and thus they attributed it to the adsorption/desorption of one hydrogen atom per step site [44,45]. However, discrepancies arose from later observations. Firstly, the interaction energy between hydrogen atoms adsorbed on the terrace is repulsive, while there is an apparent attractive interaction between the adsorbed species that give rise to the H_{upd}-step peak [66–68]. Secondly, this peak shifts with 10 mV per pH unit in RHE scale, which can not be explained with simple hydrogen adsorption/desorption [69]. Thirdly, laser-pulsed experiments revealed a change of the dipole moment from (part of) the adsorbed species at potentials around the H_{upd}-step peak [70].

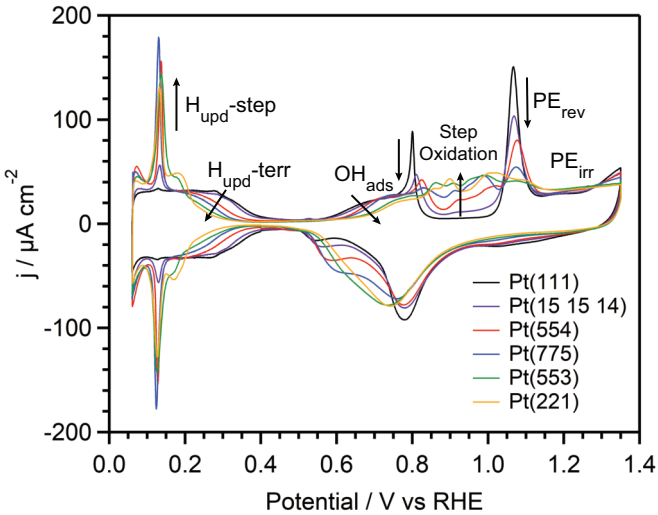

Figure 4.1: Cyclic Voltammograms of Pt(111) and its Vicinal Surfaces with (111) Steps. CVs recorded in 0.1 M $HClO_4$ from 0.06 to 1.35 V using a scan rate of 50 mV s^{-1}. The most relevant regions are indicated with the corresponding text and the general trend when increasing the step density with arrows.

To solve the above conflicts, a model was proposed in which hydroxide replaces hydrogen at the steps [67, 69]. This was supported by DFT calculations, which affirmed the stability of an OH/water structure at the steps and explained the anomalous pH dependence of the H_{upd}-step peak potential [17, 71, 72]. Moreover, Rizo et al. confirmed the presence of OH_{ad} on Pt(311) at potentials within the H_{upd} region via CO displacement and *in-situ* Raman experiments [18]. However, as shown in Chapter 3 this surface has a significant fraction of step bunches, which could lead to a preferential adsorption of OH. Therefore, the definitive confirmation if OH replaces H_{ad} at single steps would require repeating these experiments with a stable stepped surface such as Pt(554).

Independently of the above, there is not yet a consensus regarding the total charge involved in the H_{upd}-step peak [44, 45, 69, 73]. The discrepancies are partially due to the different strategies used to deconvolute the step and the terrace contributions, together with the earlier belief that the maximum H_{upd}-step charge could not exceed one electron, i.e. one hydrogen per platinum step site. In this work, we numerically fit the H_{upd}-terrace peak with a Frumkin isotherm, knowing that it describes well the hydrogen adsorption/desorption [43, 74–77]:

$$ln\left(\frac{\Theta_{H_{upd},terr}}{1-\Theta_{H_{upd},terr}}\right) = -\frac{e\,(E-E_{RHE})}{k_B\,T} - \frac{\Delta G^0_{H_{upd},terr}}{k_B\,T} - \frac{w\,\Theta_{H_{upd},terr}}{k_B\,T} \tag{4.2}$$

in which $\Theta_{H_{upd},terr}$ is the hydrogen coverage at the terrace, E is the electrode potential, E_{RHE} is the reference (RHE) potential, $\Delta G^0_{H_{upd},terr}$ is the free energy of hydrogen adsorp-

tion on the terrace, and w is the interaction energy, which is positive for repulsive interactions and negative for attractive interactions between the adsorbates. k_B, T, and e have their usual meanings: the Boltzmann constant, temperature ($T = 298$ K), and the elemental electron charge, respectively.

At potentials where hydrogen desorption occurs only on the terraces, $\Theta_{H_{upd},terr}$ is directly given by:

$$\Theta_{H_{upd},terr} = \frac{1}{Q_{H_{upd},(1e^-/terr\,site)}} \int_{E_{DL}}^{E} \frac{j_{H_{upd}}(E) - j_{DL}}{\nu}\, dE \tag{4.3}$$

where $j_{H_{upd}}(E)$ is the voltammetric current density, j_{DL} ($\approx 3\ \mu$A cm^{-2}) is the current density contribution from the double layer charging, and ν is the scan rate ($\nu = 50$ mV/s). $Q_{H_{upd},(1e^-/terr\,site)}$ is the charge density corresponding to one electron interchanged per terrace site, and is given by [44, 45]:

$$Q_{H_{upd},(1e^-/terr\,site)} = \frac{2\,(n-2)\,e}{\sqrt{3}\,d^2\left(n-\frac{2}{3}\right)} \tag{4.4}$$

where n is the number of atomic rows on a single terrace and d is the distance between two Pt atoms in the close packed (111) terrace.

Figure 4.2 shows the resulting fits of the H_{upd}-terrace peak for each of the stepped surfaces used. From 0.2 V (0.23 V for Pt(221)) there is good match between the fitted curve $j_{H_{upd},terr}$, in blue, and the experimental $j_{H_{upd}}$ curve in black, which demonstrates the validity of our fit. This is also evident from Fig. C.1 (in Appendix C), where we show the respective hydrogen coverages versus the electrode potential.

Table 1 shows $\Delta G^0_{H_{upd},terr}$ and w that we obtained in this study, together with the values reported in Ref. [43]. Both parameters decrease in absolute values with increasing step density, which is an effect of the Smoluchowski relaxation on the terraces, i.e. the terrace atoms are more compressed together, resulting in a higher driving force necessary to bind the hydrogen at the three-fold hollow sites [59–61].

	n	$\Delta G^0_{H_{upd},terr}$ / eV	w / eV
$Pt(111)$*	–	−0.289	0.286
$Pt(15\,15\,14)$	30	−0.279	0.293
$Pt(15\,15\,14)$*	30	−0.285	0.287
$Pt(554)$	10	−0.232	0.228
$Pt(775)$	7	−0.214	0.198
$Pt(553)$	5	−0.197	0.176
$Pt(553)$*	5	−0.203	0.165
$Pt(221)$	4	−0.185	0.182

Table 4.1: Thermodynamic Data for the Hydrogen Adsorption on Terraces. Free energy of hydrogen adsorption on the terrace ($\Delta G^0_{H_{upd},terr}$) and the corresponding interaction energy (w). *Reported values from Ref. [43].

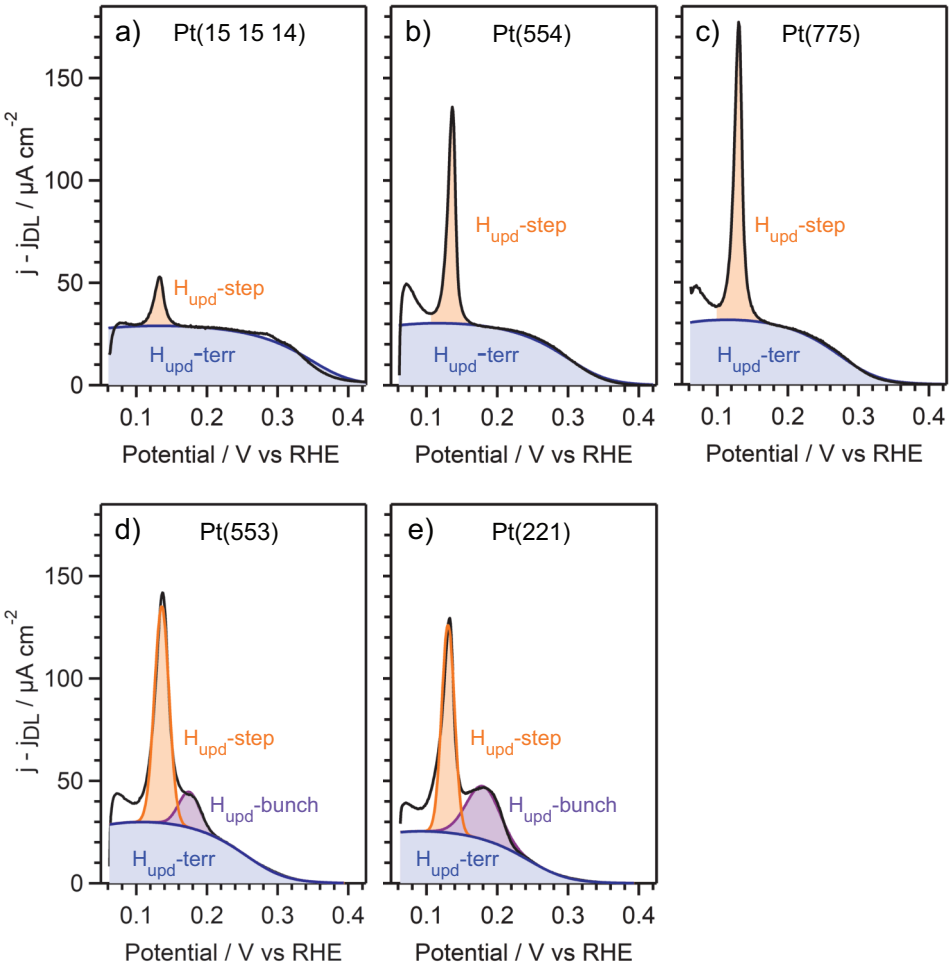

Figure 4.2: H_{upd} Deconvolution into Step and Terrace Contributions. The black line represents the total, measured H_{upd} current density after correction for the current density contribution from the double layer charging, while the blue line is the fit of the the H_{upd}-terrace current density with a Frumkin isotherm. The corresponding terrace, single step, and step bunch contributions to the H_{upd} charge density are colored in blue, orange, and purple, respectively.

Figure 4.3a shows the experimentally determined H_{upd}-terrace charge, $Q_{H_{upd},terr}$, versus the theoretical charge of one electron per terrace atom given by eq. 4.4. All the data points except for Pt(221) lie on a straight line that corresponds to a maximum hydrogen coverage of 0.67 ML. This value agrees very well with the earlier reported values for Pt(111) [74, 76], as well as for (111)-vicinal surfaces [44, 45].

Subsequently, for Pt(15 15 14), Pt(554), and Pt(775), we determined the step charge by

integrating the H_{upd}-step peak current, $j_{H_{upd},step}$, that remains after subtracting $j_{H_{upd},terr}$. We set the lower integration limit to 0.10 V to exclude the peak at 0.07 V, which is due to the oxidation of H_2 gas formed during the preceding cathodic scan (i.e. see the steep rise at 0.06 V in Fig. 4.1). For Pt(553) and Pt(221), we deconvoluted the single-step and the step-bunch peaks with Gaussians. Figure 4.3b shows the resulting H_{upd}-step (in orange), H_{upd}-bunch (in purple), and total step (in red) charges plotted versus the theoretical charge assuming one electron interchanged per unit step length, which is given by [44, 45]:

$$Q_{Hupd,(1e^-/unit\,step\,length)} = \frac{2\,e}{\sqrt{3}\,d^2\left(n-\frac{2}{3}\right)} \tag{4.5}$$

For Pt(15 15 14), Pt(554), and Pt(775), we obtained 1.30 electrons per unit step length from the slope of the linear regression. This result is close to the 1.2 electrons per unit step length reported in Ref. [73], but significantly larger than the 1.0 electrons per unit step length found by Clavilier et al. [44, 45]. The differences are probably due to the different methodology used to deconvolve the H_{upd} terrace and step contribution. Our results show that the H_{upd}-step peak does not involve the simple desorption of one hydrogen per platinum step atom, as this would result in exactly 1.0 electrons per unit step length. Although it is not a proof, the charge obtained of 1.30 electrons per unit step length could be explained by the exchange mechanism proposed in the literature [17, 18, 67, 69–72], in which hydrogen is (partially) replaced by hydroxide. Following this argument, 1.0 electrons would be attributed to hydrogen desorption and 0.3 electrons to hydroxide adsorption, resulting in 0.3 ML OH adsorbed at the steps at potentials more positive than the H_{upd}-step peak. This would agree with DFT calculations, which show that low $OH_{ad,\,step}$ coverages, e.g. 1/3 ML, are the most favorable thermodynamically, as the co-adsorption of water is necessary to stabilize the adsorbed structure [17, 71, 72].

For Pt(553) and Pt(221) the normalized total H_{upd}-step charge is lower: 1.21 and 1.06 electrons per unit step length, respectively (see Fig. 4.3b). This is because these surfaces present not only single steps, but an even larger fraction of step bunches. Concretely, in Chapter 3 we quantified with EC-STM that Pt(553) has 35±4 % of single steps, 51±5 % of double steps, and 14±3 % of triple steps. As illustrated in Fig. 4.4, (111)-step bunches consist of an upper and a lower step edge as well as a {111} facet. As the latter is not present on single steps, it must be the reason for the (extra) H_{upd}-bunch peak on Pt(553) and Pt(221), shown in Fig. 4.2. On Pt(553), the H_{upd}-bunch peak involves a charge of 0.23 electrons per unit step length. Knowing that this charge must originate from the {111} facets at double and triple steps, from which we know their percentages, we calculated that only 0.67±0.04 electrons are interchanged per facet site. This is only half of the 1.30 electrons transferred per unit step length at single steps, and thereby it explains the decrease of the (normalized) total H_{upd}-step charge due to step bunching.

Similarly, as the upper and lower step edges from single steps are geometrically equal to the ones from bunched steps, we can calculate the charge expected for the H_{upd}-step peak of Pt(553). Knowing that 1.30 electrons are interchanged per unit step length at single step sites, as well as the percentage of single, double, and triple steps, we obtained 0.85±0.03 electrons per unit step length. This value is not too far from the one measured of 0.98 electrons per unit step length, shown in orange in Fig. 4.3b.

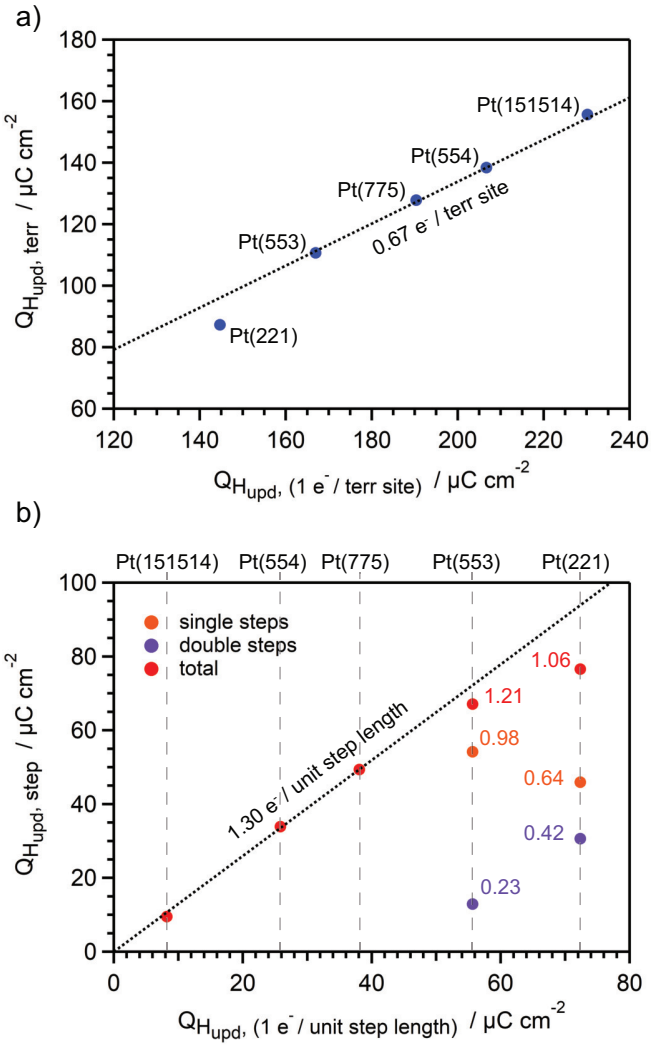

Figure 4.3: Correlation between the Measured and the Theoretical H_{upd} Charge Densities on Terraces and Steps. (a) H_{upd} charge densities on terraces, as given by a Frumkin isotherm fit, versus the theoretical charge densities assuming one electron is transferred per terrace site. **(b)** H_{upd} charge densities from single steps (orange), step bunches (purple), and the sum of them (red), versus the theoretical charge densities assuming one electron is interchanged per unit step length. We also provide the experimental values in units of electrons per unit step length.

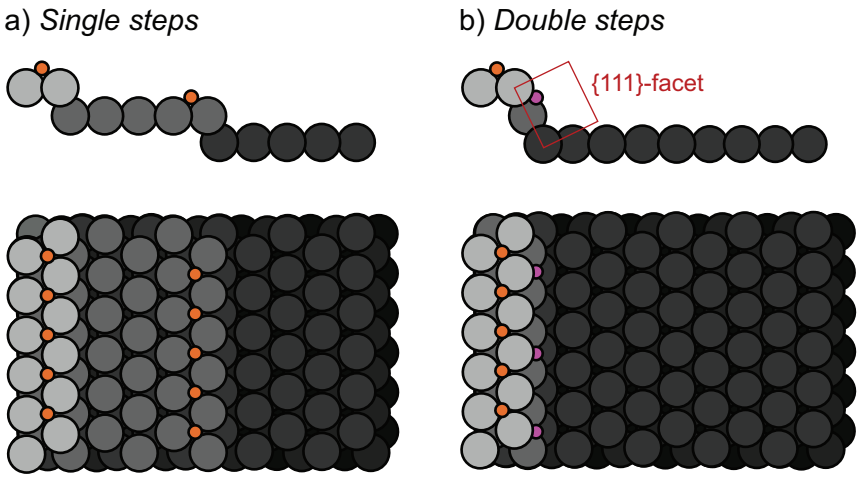

Figure 4.4: Hydrogen Adsorption at Single and Bunched Steps. (a) Hydrogen adsorption on a (111) single step and **(b)** on a double (bunched) step. For the single step site, we have drawn the hydrogen adsorbed at fcc sites at the upper step edge (in orange), although this is not clear from DFT calculations due to the similar binding energies between the fcc, hcp, and bridge sites [52, 71]. Moreover, from our quantitative analysis we can not discard that the step sites related to the H_{upd}-step peak are located, instead, at the lower step edge, as this would result in the same H_{upd}-step charge. On step bunches hydrogen adsorbs, in addition, at the {111}-facet formed (in purple), although we know from the charge density analysis that some of these sites must remain unoccupied. A triple step (not shown here) presents one row of fcc adsorption sites at the upper step edge and two rows at the {111}-facet.

4.5 Adsorption of Oxygen at Step Sites

Based on Fig. 4.1 and Refs. [30, 51], we know that step oxidation occurs between 0.85 and 1.05 V and it involves three voltammetric peaks with unknown charge density. We therefore fit these peaks with Gaussian functions, which is a decent approximation to the Frumkin isotherm [78, 79]. In order to determine the lower and upper boundaries for the fit, we plotted the Chi Squared versus the lower and upper fit potential and choose for the inflection points where the Chi Squared begins to plateau (see Figs. C2 and C.3 in Appendix C).

Figure 4.5 shows, for each of the stepped surfaces, the deconvolution with the three step oxidation Gaussians (in purple, orange, and blue) as well as an additional one for the PE_{rev}-peak (in green). The yellow and gray curves are attributed to OH adsorption and to the PE_{irr} regime, respectively, and result naturally when subtracting the Gaussian fits from the total current density.

Figure 4.6 (a-c) shows the individual step oxidation charges, $Q_{PtOx,step}$, from each of the Gaussians, plotted versus the step density, while Fig. 4.6d shows the total, combined step oxidation charge. Each trend line relates to a different number of electrons transferred per

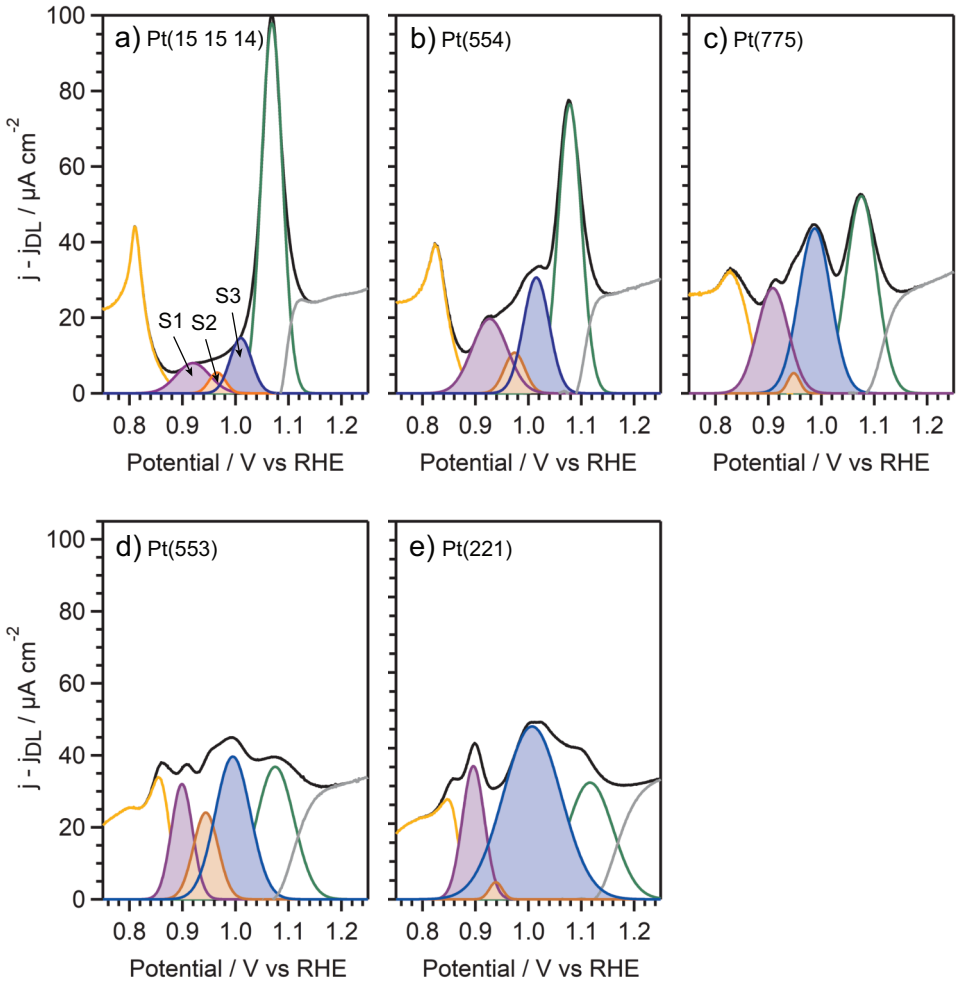

Figure 4.5: Deconvolution of the Platinum Oxidation Region: the three step oxidation peaks (S1, S2, and S3, respectively) as well as the PE_{rev}-peak (green curve) are obtained with Gaussian fit functions. The OH_{ads} butterfly peak in yellow and the PE_{irr}-peak in gray are derived by subtraction of the Gaussian peaks from the measured total current density, shown in black.

unit of step length, $q_{PtOx,step}$, which we calculated with:

$$q_{PtOx,step} = \frac{\sqrt{3}\,d^2}{2\,e}\,b \tag{4.6}$$

where b is the slope of the given trend line. For the sake of simplicity, we have provided the values of $q_{PtOx,step}$ (and not b) next to each of the trend lines. Alternatively, we could have also calculated $q_{PtOx,step}$ for each individual data point, knowing that:

$$Q_{PtOx,\,step} = \frac{q_{PtOx,\,step}\,2\,e}{\sqrt{3}\,d^2}\,\frac{1}{n-\frac{2}{3}} \tag{4.7}$$

Interestingly, Fig. 4.6a as well as Fig. 4.6d show two different trends, indicating a different degree of oxidation between single steps and bunched steps, which are in our case mainly double steps. We will discuss this in more depth at the end of this section, and will focus now on identifying the specific processes that give rise to each of the step oxidation peaks (see Fig. 4.7a) and their relation to specific atomic sites.

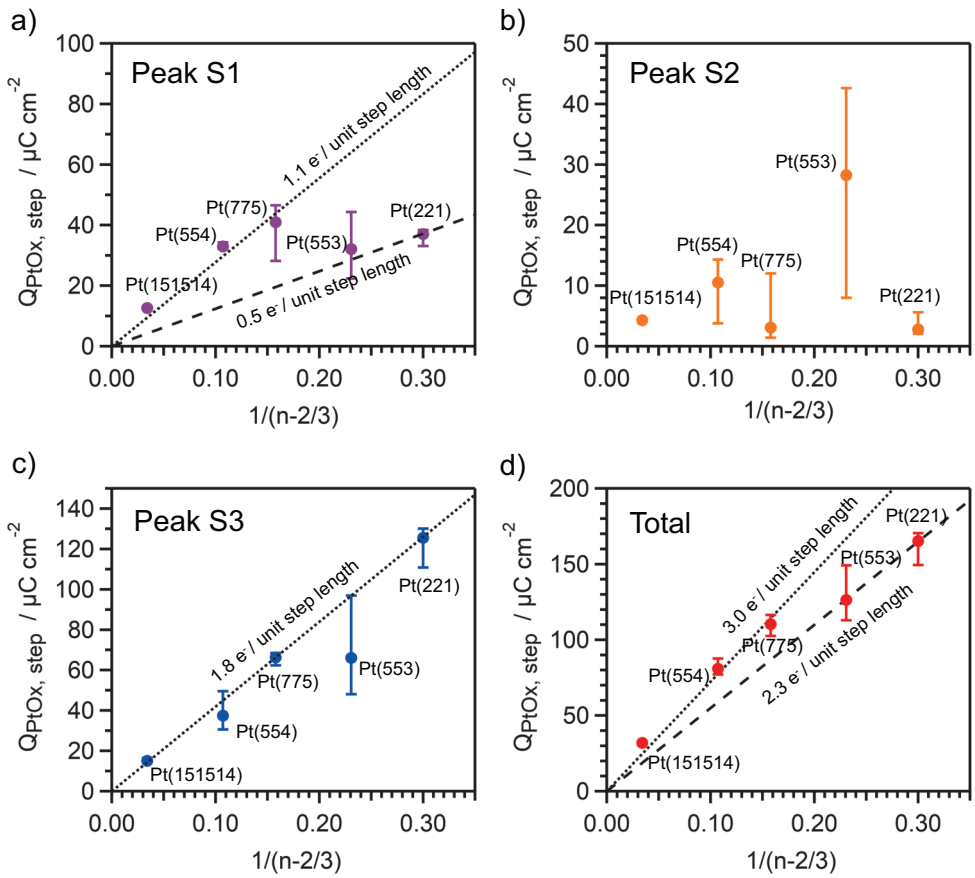

Figure 4.6: Step Oxidation Charges versus Step Density: **(a-c)** step oxidation charges resulting from the integral of each of the step oxidation peaks fitted in Fig. 4.5, as indicated. **(d)** shows the total step oxidation charge, which is the sum of the three peaks. We also show the resulting numbers of electrons transferred per unit step length for each peak, which we calculated from the trend lines. In **(a)** and **(d)**, two different regimes are clearly visible: one involving Pt(15 15 14), Pt(554), and Pt(775), and the other involving Pt(553) and Pt(221). The reason for the two regimes is step bunching. The error bars show the variation of the corresponding charges when taking sub-optimal fits (i.e. with a higher Chi Squared) obtained when varying slightly the upper and lower fitting boundaries.

Björling and co-workers found a step oxidation charge of around 2 electrons per unit step length for Pt(775) in 5 mM H_2SO_4 [30], and thus concluded that PtO forms, according to:

$$Pt^*_{step} + H_2O \rightleftharpoons PtOH_{step} + H^+ + e^- \tag{4.8}$$

$$PtOH_{step} \rightleftharpoons PtO_{step} + H^+ + e^- \tag{4.9}$$

In comparison with our results, Fig. 4.6d shows that step oxidation on Pt(15 15 14), Pt(554), and Pt(775) involves around 3.0 electrons per unit step length. This suggests that the oxidation proceeds further towards PtO_2:

$$PtO_{step} + H_2O \rightleftharpoons PtO_{2,\,step} + 2\,H^+ + 2\,e^- \tag{4.10}$$

However, the complete oxidation of the steps to PtO_2 (eq. 4.8-4.10) would require 4 electrons per unit step length, and not only 3. There are several explanations for this. Firstly, if true that 0.3 ML OH adsorbs at the steps within the H_{upd}-step peak, as discussed in the last section, the step oxidation charge expected in the platinum oxidation region must decrease by 0.3 electrons per unit step length. Moreover, we can not discard that part of the adsorption of OH at steps is convoluted with the one at the terraces, and thus the steps might be covered with 1 ML OH_{ad} before entering the step oxidation region. We would overlook this charge in our quantification.

The formation of PtO_2 at steps is supported by DFT, Force Field, and X-Ray Spectroscopy studies in vacuum, which all agree that, at high oxygen chemical potential, two oxygen atoms adsorb for each Pt step atom, resulting in a one-dimensional PtO_2 structure along the step [39–41]. Interestingly, there are indications for similar oxide chain structures on the (111) terraces [26, 27, 40, 51, 58, 62, 80, 81].

The formation of PtO_2 requires at least two geometrically different adsorption sites at the (111) step edge, as it involves adsorbing two oxygen atoms to one step platinum atom [40]. In an STM study, Feibelman and co-workers showed that, at low coverages, O adsorbs at the upper terrace on the fcc sites (see purple atoms in Fig. 4.7b) [82], which is not surprising as, at low coverages, oxygen adsorbs also on fcc sites on the terraces [83]. Upon increasing oxygen coverage, the chemical potential increases, resulting in the formation of one-dimensional PtO_2 chains along both (111) and (100) type of steps [39–41]. For (111) steps, the required second oxygen atom adsorbs at the lower step edge (partially subsurface), just on top of the lower step edge atom, as indicated in Fig. 4.7b with the blue atoms [40]. Knowing that this subsurface site is only occupied at higher oxygen coverages, the corresponding voltammetric peak must also appear at higher potentials.

Keeping the above in mind, we attribute the S1 peak in Fig. 4.7a to oxygen adsorbing at the upper part of the step, while the S3 peak must come from the lower, partial subsurface adsorption. This implies that the adsorption of OH (equation 4.8) is coupled with its oxidation to $O_{ad,\,step}$ (equation 4.9), giving rise to only one voltammetric peak, S1. Alternatively, one could think that this first peak is attributed to the OH adsorption at both the upper and the lower parts of the step, while the S3 peak would relate to the further oxidation towards $O_{ad,\,step}$. Both possibilities would result in a charge equivalent to 2.0 electrons per unit step length for both the S1 and the S3 peak. Therefore, we can not discard any of them from our quantitative analysis, which on surfaces with (predominantly) single steps deliver 1.1

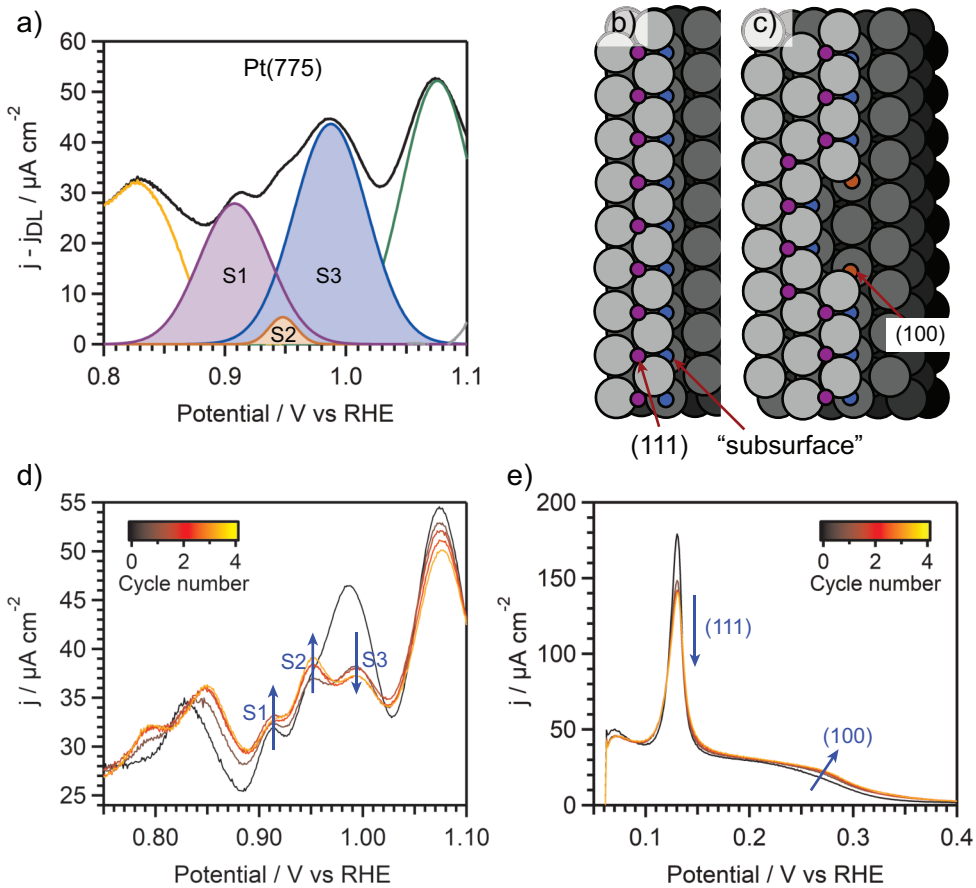

Figure 4.7: Atomic Site Identification of the Step Oxidation Peaks. **(a)** Step oxidation peaks of Pt(775). **(b)** Corresponding oxygen adsorption sites at the (111) (fcc) position at the upper step edge and the threefold subsurface position at the lower step edge. **(c)** Oxygen adsorption sites at a faceted (111) step with (100) microfacets, which present a partially subsurface site with twofold coordination at the lower step edge. **(d)** Step oxidation peaks upon oxidation-reduction cycling: S1 and S2 increase in intensity due to the increase in the number of (111) and (100) sites, respectively, while S3 decreases due to the annihilation of subsurface sites at the lower (111)-step edge. **(e)** H_{upd} region upon oxidation-reduction cycling: the (100) step peak increases at the expense of the (111) step peak during the first 5 cycles.

and 1.8 electrons per unit step length, respectively (see Fig. 4.6a and 4.6c). The fact that the former value is much lower than the expected 2.0 electrons per unit step length stems from one of the explanations given above regarding the total step oxidation charge. If the steps would be already covered with hydroxide before reaching the step oxidation region, we would expect the S1 peak to exhibit a charge of 1.0 electrons per unit step length, which is close to the value we measured.

The S2 peak represents only a low percentage of the total step oxidation charge, except on Pt(553), where the error bar is large. Therefore, we assigned this peak to oxygen adsorption at (100) microfacets that are formed due to the presence of kinks (see Fig. 4.7c). The concentration of kinks, and thus of (100) microfacets, is naturally given by the temperature and the kink formation energy (see Appendix C) [8]. However, this concentration can increase due to the adsorption of species like hydrogen and oxygen. The former can induce the "roughening" of (111) steps into triangular microfacets composed by (100)-steps [84], while the oxidation of steps results in their decomposition into clusters with predominantly (111) microfacets [63, 64, 85–88]. This latter process is primarily driven by the buckling of the step atoms [89–91], which can even be pushed out onto the upper terrace in order to compensate for the high repulsive-interaction between the oxygen atoms as well as for the lattice mismatch between PtO_2 and platinum [58, 62, 80].

Figure 4.7d shows the evolution of the step oxidation region upon oxidation-reduction cycling between 0.06 V to 1.35 V, which leads to faceting and ultimately to the fragmentation of the (111) steps into clusters [88]. This results in an increase of the (100) step length at the expense of the (111) steps, as evident from the evolution of the respective peaks in the well-known H_{upd} region [46, 63, 64, 87], shown in Fig. 4.7e, and from the counting of the blue atoms in Fig. 4.7c. As only the S3 peak in Fig. 4.7d decreases in intensity with cycle number, it must be attributed to a surface site that disappears during this process: the partially subsurface sites at the lower (111) step edge, as we assigned earlier. We also related the S1 peak to the (111) sites at the upper terrace, which grow in number during oxidation-reduction cycling due to the increase of the total step length (note from Fig. 4.7d that both (111) and (100) microfacets present these O adsorption sites [39–41]). In each oxidation-reduction cycle the steps become more faceted, and thus have a larger fraction of (100) microfacets. Therefore, the rise of the S2 peak is attributed to the increase of the partially subsurface sites at the (100) step edges (see orange atoms in Fig. 4.7c).

Finally, we discuss how step bunching can explain the decreased step oxidation charges for Pt(553) and Pt(221), as shown in Fig. 4.6. Figure 4.8a and 4.8b represent the oxygen adsorption on a Pt(553) surface with single steps and with double steps, respectively. While single steps accommodate (at most) 2 rows of oxygen each (in purple and blue), and thus a total of 4 rows in this picture, only 3 oxygen rows can adsorb at double steps. This is a factor 1/4 less, which is the same that we find when comparing the two regimes in Fig. 4.6d: 3.0 electrons per unit step length on surfaces with single steps and 2.3 electrons per unit step length on surfaces with mainly double steps. As we know from EC-STM measurements that Pt(553) has actually 35±4 % of single steps, 51±5 % of double steps, and 14±3 % of triple steps (see Chapter 3), we can calculate more precisely the expected step oxidation charge. Assuming also that four oxygen rows adsorb on each triple step (not shown in Fig. 4.8), we obtain a value of 2.48±0.05 electrons per unit step length, which is close to the value of 2.3 electrons per unit step unit length shown in Fig. 4.6d for Pt(553). From Fig. 4.8 it is also evident that the lower step oxidation charge on surfaces with mainly step bunches originates from a decrease in the number of (111) sites at the upper step edge (purple atoms). This is also reflected in Fig. 4.6a, which shows that the oxidation of these sites on Pt(553) and Pt(221) involves about half of the number of electrons per unit step length compared to Pt(15 15 14), Pt(554), and Pt(775). From the measured fraction of step

bunches on Pt(553), we expect 0.70±0.03 electrons per unit step length on Pt(553). Lastly, the number of adsorption sites at the lower step edge (blue atoms) does not change due to step bunching, which explains that we only observe one trend in Fig. 4.6c.

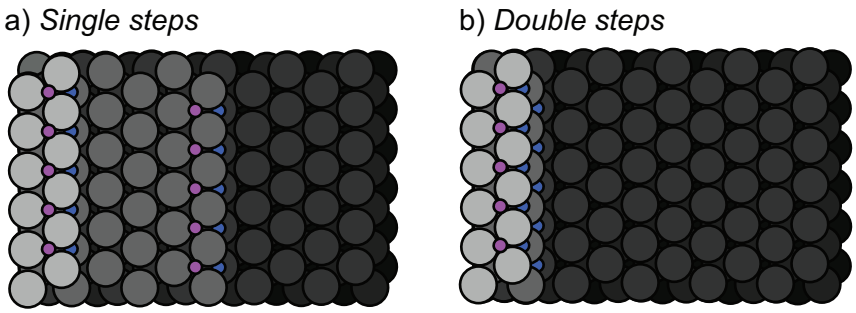

Figure 4.8: Oxidation of Single and Double Steps. **(a)** PtO_2 structure on single steps of Pt(553). The purple and blue oxygen circles represent oxygen atoms adsorbed at (111) (fcc) sites on the upper step edge and partially subsurface sites on the lower step edge, respectively. **(b)** PtO_2 structure on double steps of Pt(553). One row of O_{ad} at the upper step edge is missing in comparison to the single step structure.

4.6 Conclusions

In the present study, we used platinum (111)-vicinal surfaces to quantify the adsorption of H and O at step sites. For each of the stepped surfaces used, we fitted the H_{upd}-terrace peak with the Frumkin isotherm in order to deconvolute it from the H_{upd}-step peak. The subsequent charge analysis of both voltammetric peaks concludes that 0.67 electrons are transferred per terrace site on Pt(15 15 14), Pt(554), Pt(775), and Pt(553), while this charge is lower for Pt(221). We also found that 1.3 electrons are transferred per unit step length for Pt(15 15 14), Pt(554), Pt(775), which supports that the H_{upd}-step peak does not involve simple desorption of one hydrogen per step atom site, as this would imply exactly 1.0 electrons per unit step length. A possible explanation to the higher charge within this peak could be that it involves the (partial) replacement of $H_{ad,\,step}$ by $OH_{ad,\,step}$, as proposed in the most recent literature. On the other hand, we only quantified 1.21 and 1.06 electrons per unit step length for the step contribution on Pt(553) and Pt(221), respectively. This lower charge is attributed to the large fraction of step bunches on Pt(553) and Pt(221), which even give rise to an extra peak, the H_{upd} step-bunch peak, not present on stable (111)-vicinal surfaces.

At higher electrode potentials (between 0.85 V and 1.05 V), the steps oxidize, giving rise to three peaks. For Pt(15 15 14), Pt(554), and Pt(775), these three peaks imply a total (combined) charge of around 3.0 electrons per unit step length, while only 2.3 electrons per unit step length for Pt(553) and Pt(221). Although we can not discard that part of the step oxidation charge might be convoluted with the $OH_{ad,\,terr}$ region at around 0.7 V, our results indicate that the oxidation process results in PtO_2 chains along the steps. This agrees well

with DFT calculations and XPS measurements in vacuum, as well as with the oxide spokes observed (also in vacuum) on platinum terraces. Based on our new understanding, we identified the specific step sites where oxygen adsorbs giving rise to each of the three step oxidation peaks. From stronger to weaker oxygen binding, i.e. lower to higher peak potentials in the CV, these sites are: the (111) (fcc hollow) sites at the upper edge of the step, the (100) step sites that result from faceted (111) steps, and the partially subsurface sites at the lower step edge. Finally, we showed quantitatively that the decreased step oxidation charge that we found on Pt(553) and Pt(221) stems from the large fraction of bunched steps, which decreases the number of available (111) sites at the upper step edge where oxygen can adsorb.

References

[1] B. E. Conway, B. V. Tilak, *Electrochim. Acta*, **47**, 3571 (2002).

[2] J. K. Nørskov, T. Bligaard, A. Logadottir, J. R. Kitchin, J. G. Chen, S. Pandelov, and U. Stimming, *J. Electrochem. Soc.*, **152**, J23 (2005).

[3] G. Jerkiewicz, *Prog. Surf. Sci.*, **57**, 137 (1998).

[4] M. Luo and M. T. M. Koper, *Nat. Catal.*, **5**, 615 (2022).

[5] N. P. Lebedeva, M. T. M. Koper, E. Herrero, J. M. Feliu, and R. A. van Santen, *J. Electroanal. Chem.*, **487**, 37 (2000).

[6] A. Frumkin and B. Slygin, *Acta Physicochim. U.R.S.S*, **5**, 819 (1936).

[7] D. M. Kolb, M. Przasnyski, and H. Gerischer, *J. Electroanal. Chem.*, **54**, 25 (1974).

[8] H. Ibach, *Physics of Surfaces and Interfaces*, Springer, Amsterdam (2006).

[9] J. Clavilier, R. Faure, G. Guinet, and R. Durand, *J. Electroanal. Chem.*, **107**, 205 (1980).

[10] N. Furuya and S. Koide, *Surf. Sci.*, **220**, 18 (1989).

[11] F. Calle-Vallejo, J. Tymoczko, V. Colic, Q. Huy Vu, M. D. Pohl, K. Morgenstern, D. Loffreda, P. Sautet, W. Schuhmann, and A. S. Bandarenka, *Science*, **350**, 185 (2015).

[12] C. L. Scortichini and C. N. Reilley, *J. Electroanal. Chem.*, **139**, 233 (1982); C. L. Scortichini and C. N. Reilley, *J. Electroanal. Chem.*, **139**, 247 (1982).

[13] D. Armand and J. Clavilier, *J. Electroanal. Chem.*, **225**, 205 (1987); D. Armand and J. Clavilier, *J. Electroanal. Chem.*, **233**, 251 (1987).

[14] P. N. Ross, *Surf. Sci.*, **102**, 463 (1981).

[15] J. Clavilier, D. Armand, S. G. Sun, and M. Petit, *J. Electroanal. Chem.*, **205**, 267 (1986).

[16] S. Motoo and N. Furuya, *Ber. Bunsenges. Phys. Chem.*, **91**, 457 (1987).

[17] I. T. McCrum, X. Chen, K. A. Schwarz, M. J. Janik, and M. T. M. Koper, *J. Phys. Chem. C*, **122**, 16756 (2018).

[18] R. Rizo, J. Fernández-Vidal, L. J. Hardwick, G. A. Attard, F. J. Vidal-Iglesias, V. Climent, E. Herrero, and J. M. Feliu, *Nat. Commun.*, **13**, 2550 (2022).

[19] A. M. Gómez-Marín, J. Clavilier, and J. M. Feliu, *J. Electroanal. Chem.*, **688**, 360 (2013).

[20] H. Javed, A. Knop-Gericke, and R. V. Mom, *ACS Appl. Mater. Interfaces*, **14**, 36238 (2022).

[21] M. A. H. Lanyon and B. M. W. Trapnell, *Proc. R. Soc. A.*, **227**, 387 (1955).

[22] A. K. N. Reddy, M. A. Genshaw, and J. O. Bockris, *J. Chem. Phys.*, **48**, 671 (1968).

[23] K. J. Vetter and J. W. Schultze, *J. Electroanal. Chem.*, **34**, 141 (1972).

[24] B. V. Tilak, B. E. Conway, and H. Angerstein-Kozlowska, *J. Electroanal. Chem.*, **48**, 1 (1973).

[25] G. Jerkiewicz, G. Vatankhah, J. Lessard, M. P. Soriaga, and Y. Park, *Electrochim. Acta*, **49**, 1451 (2004).

[26] L. Jacobse, V. Vonk, I. T. McCrum, C. Seitz, M. T. M. Koper, M. J. Rost, and A. Stierle, *Electrochim. Acta*, **407**, 139881 (2022).

[27] M. J. Rost, *J. Electrochem. Soc.*, **170**, 012504 (2023).

[28] H. Angerstein-Kozlowska, B. E. Conway, and W. B. A. Sharp, *J. Electroanal. Chem.*, **43**, 9 (1973).

[29] A. Björling, E. Ahlberg, and J. M. Feliu, *Electrochem. Commun.*, **12**, 359 (2010).

[30] A. Björling, E. Herrero, and J. M. Feliu, *J. Phys. Chem.*, **115**, 15509 (2011).

[31] J. K. Nørskov, J. Rossmeisl, A. Logadottir, L. Lindqvist, J. R. Kitchin, T. Bligaard, and H. Jónsson, *J. Phys. Chem. B*, **108**, 17886 (2004).

[32] N. Hoshi, M. Nakamura, and A. Hitotsuyanagi, *Electrochim. Acta*, **112**, 899 (2013).

[33] A. S. Bandarenka, H. A. Hansen, J. Rossmeisl, and I. E. L. Stephens, *Phys. Chem. Chem. Phys.*, **16**, 13625 (2014).

[34] T. Iwasita, *Electrochim. Acta*, **47**, 3663 (2002).

[35] A. A. Topalov, S. Cherevko, A. R. Zeradjanin, J. C. Meier, I. Katsounaros, and K. J. J. Mayrhofer, *Chem. Sci.*, **5**, 631 (2014).

[36] D. J. S. Sandbeck, M. Inaba, J. Quinson, J. Bucher, A. Zana, M. Arenz, and S. Cherevko, *ACS Appl. Mater. Interfaces*, **12**, 25718 (2020).

[37] T. Michely and J. Krug, *Islands, Mounds and Atoms*, Springer, Amsterdam (2004).

[38] E. Hahn, H. Schief, V. Marsico, A. Fricke, and K. Kern, *Phys. Rev. Lett.*, **72**, 3378 (1994).

[39] J. G. Wang, W. X. Li, M. Borg, J. Gustafson, A. Mikkelsen, T. M. Pedersen, E. Lundgren, J. Weissenrieder, J. Klikovits, M. Schmid, B. Hammer, and J. N. Andersen, *Phys. Rev. Lett.*, **95**, 256102 (2005).

[40] J. Bandlow, P. Kaghazchi, and T. Jacob, *Phys. Rev. B*, **83**, 174107 (2011).

[41] D. Fantauzzi, J. Bandlow, L. Sabo, J. E. Mueller, A. C. T. van Duin, and T. Jacob, *Phys. Chem. Chem. Phys.*, **16**, 23118 (2014).

[42] A. Farkas, D. Fantauzzi, J. E. Mueller, T. Zhu, C. Papp, H. Steinrück, and T. Jacob, *J. Electron Spectrosc. Relat. Phenom.*, **221**, 44 (2017).

[43] A. M. Gómez-Marín and J. M. Feliu, *Surf. Sci.*, **646**, 269 (2016).

[44] J. Clavilier, K. El Achi, and A. Rodes, *J. Electroanal. Chem.*, **272**, 253 (1989).

[45] J. Clavilier, K. El Achi, and A. Rodes, *Chem. Phys.*, **141**, 1 (1990).

[46] A. Rodes, K. El Achi, M. A. Zamakhchari, and J. Clavilier, *J. Electroanal. Chem.*, **284**, 245 (1990).

[47] S. Taguchi and J. M. Feliu, *Electrochim. Acta*, **52**, 6023 (2007).

[48] M. T. M. Koper and J. J. Lukkien, *J. Electroanal. Chem.*, **485**, 161 (2000).

[49] A. M. Gómez-Marín and J. M. Feliu, *Electrochim. Acta.*, **104**, 367 (2013).

[50] T. Fuchs, V. Briega-Martos, J. O. Fehrs, C. Qiu, M. Mirolo, C. Yuan, S. Cherevko, J. Drnec, O. M. Magnussen, and D. A. Harrington, *J. Phys. Chem. Lett.*, **14**, 3589 (2023).

[51] F. Valls Mascaró, I. T. McCrum, M. T. M. Koper, and M. J. Rost, *J. Electrochem. Soc.*, **169**, 112506 (2022).

[52] M. J. Kolb, F. Calle-Vallejo, L. B. F. Juurlink, and M. T. M. Koper, *J. Chem. Phys.*, **140**, 134708 (2014).

[53] M. Wakisaka, H. Suzuki, S. Mitsui, H. Uchida, and M. Watanabe, *Langmuir*, **25**, 1897 (2009).

[54] H. You, D. J. Zurawski, Z. Nagy, and R. M. Yonco, *J. Chem. Phys.*, **100**, 4699 (1994).

[55] Y. Liu, A. Barbour, V. Komanicky, and H. You, *J. Phys. Chem. C*, **120**, 16174 (2016).

[56] J. Drnec, M. Ruge, F. Reikowski, B. Rahn, F. Carlà, R. Felici, J. Stettner, O. M. Magnussen, and D. A. Harrington, *Electrochim. Acta*, **224**, 220 (2017).

[57] M. Ruge, J. Drnec, B. Rahn, F. Reikowski, D. A. Harrington, F. Carlà, R. Felici, J. Stettner, and O. M. Magnussen, *J. Electrochem. Soc.*, **164**, H608 (2017).

[58] M. J. Rost, L. Jacobse, and M. T. M. Koper, *Angew. Chem. Int. Ed.*, **62**, e202216376 (2023).

[59] R. Smoluchowski, *Phys. Rev.*, **60**, 661 (1941).

[60] K. H. Lau and W. Kohn, *Surf. Sci.*, **65**, 607 (1977).

[61] V. I. Marchenko and A. Ya. Parshin, *Sov. Phys. JETP*, **52**, 129 (1980).

[62] S. Hanselman, I. T. McCrum, M. J. Rost, and M. T. M. Koper, *Phys. Chem. Chem. Phys.*, **22**, 10634 (2020).

[63] L. Jacobse, Y. F. Huang, M. T. M. Koper, and M. J. Rost, *Nat. Mater.*, **17**, 277 (2018).

[64] L. Jacobse, M. J. Rost, and M. T. M. Koper, *ACS Cent. Sci.*, **5**, 1920 (2019).

[65] M. J. Rost, L. Jacobse, and M. T. M. Koper, *Nat. Commun.*, **10**, 5233 (2019).

[66] B. Love, K. Seto, and J. Lipkowski, *J. Electroanal. Chem.*, **199**, 219 (1986).

[67] K. J. P. Schouten, M. J. T. C. van der Niet, and M. T. M. Koper, *Phys. Chem. Chem. Phys.*, **12**, 15217 (2010).

[68] M. T. M. Koper, J. J. Lukkien, N. P. Lebedeva, J. M. Feliu, and R. A. van Santen, *Surf. Sci.*, **478**, L339 (2001).

[69] M. J. T. C. van der Niet, N. Garcia-Araez, J. Hernández, J. M. Feliu, and M. T. M. Koper, *Catal. Today*, **202**, 105 (2013).

[70] N. García-Aráez, V. Climent, and J. M. Feliu, *Electrochim. Acta*, **54**, 966 (2009).

[71] I. T. McCrum and M. J. Janik, *ChemElectroChem*, **3**, 1609 (2016).

[72] X. Chen, I. T. McCrum, K. A. Schwarz, M. J. Janik, and M. T. M. Koper, *Angew. Chem. Int. Ed.*, **56**, 15025 (2017).

[73] I. T. McCrum and M. J. Janik, *J. Phys. Chem. C*, **121**, 6237 (2017).

[74] N. M. Marković, T. J. Schmidt, B. N. Grgur, H. A. Gasteiger, R. J. Behm, and P. N. Ross, *J. Phys. Chem.*, **103**, 8568 (1999).

[75] A. Zolfaghari, M. Chayer, and G. Jerkiewicz, *J. Electrochem. Soc.*, **144**, 3034 (1997).

[76] R. Gómez, J. M. Orts, B. Álvarez-Ruiz, and J. M. Feliu, *J. Phys. Chem. B*, **108**, 228 (2004).

[77] N. Garcia-Araez, V. Climent, and J. M. Feliu, *J. Electroanal. Chem.*, **649**, 69 (2010).

[78] E. Laviron, *J. Electroanal. Chem.*, **100**, 263 (1979).

[79] J. Solla-Gullón, P. Rodríguez, E. Herrero, A. Aldaz, and J. M. Feliu, *Phys. Chem. Chem. Phys.*, **10**, 1359 (2008).

[80] M. A. van Spronsen, J. W. M. Frenken, and I. M. N. Groot, *Nat. Commun.*, **8**, 429 (2017).

[81] D. Boden, I. M. N. Groot, and J. Meyer, *J. Phys. Chem. C*, **126**, 20020 (2022).

[82] P. J. Feibelman, S. Esch, and T. Michely, *Phys. Rev. Lett.*, **77**, 2257 (1996).

[83] K. Mortensen, C. Klink, F. Jensen, F. Besenbacher, and I. Stensgaard, *Surf. Sci.*, **220**, L701 (1989).

[84] I. T. McCrum, C. J. Bondue, and M. T. M. Koper, *J. Phys. Chem. Lett.*, **10**, 6842 (2019).

[85] Z. Zhu, F. F. Tao, F. Zheng, R. Chang, Y. Li, L. Heinke, Z. Liu, M. Salmeron, and G. A. Somorjai, *Nano Lett.*, **12**, 1491 (2012).

[86] Z. Zhu, G. Melaet, S. Axnanda, S. Alayoglu, Z. Liu, M. Salmeron, and G. A. Somorjai, *J. Am. Chem. Soc.*, **135**, 12560 (2013).

[87] A. Björling and J. M. Feliu, *J. Electroanal. Chem.*, **662**, 17 (2011).

[88] F. Valls Mascaró, M. T. M. Koper, and M. J. Rost, in preparation.

[89] S. Helveg, H. T. Lorensen, S. Horch, E. Lægsgaard, I. Stensgaard, K. W. Jacobsen, J. K. Nørskov, and F. Besenbacher, *Surf. Sci.*, **430**, L533 (1999).

[90] J. Xu, W. Xie, Y. Han, and P. Hu, *ACS Catal.*, **12**, 14812 (2022).

[91] N. Fukaya, H. Murata, M. Shibata, and R. Jinnouchi, *Electrochim. Acta*, **464**, 142867 (2023).